



Analyst

Identification of early inflammatory changes in the tympanic membrane with Raman spectroscopy

Journal:	<i>Analyst</i>
Manuscript ID	AN-ART-09-2019-001772.R1
Article Type:	Paper
Date Submitted by the Author:	04-Oct-2019
Complete List of Authors:	Singh, Surya Pratap; Massachusetts Institute of Technology, Chemistry; Stanford University School of Medicine, Otolaryngology Xia, Anping; Stanford University School of Medicine, Otolaryngology Tusty, Mahbuba; Stanford University School of Medicine, Otolaryngology Malkovskiy, Andrey; Stanford University School of Medicine, Easwaran, Meena; Stanford University School of Medicine, Otolaryngology Zarabanda, David; Stanford University School of Medicine, Otolaryngology Valdez, Tulio; Stanford University School of Medicine, Otolaryngology

SCHOLARONE™
Manuscripts

1
2
3 Identification of early inflammatory changes in the tympanic membrane with
4 Raman spectroscopy
5

6 S.P.Singh¹, Anping Xia¹, Mahbuba Tusty¹, Andrey Victorovich Malkovskiy², Meena Easwaran¹,
7 David Zarabanda¹, Tulio A Valdez^{1*}
8
9

10 ¹ Department of Otolaryngology and Head and Neck Surgery, School of Medicine, Stanford
11 University, Palo Alto, CA, 94305, USA
12

13 ² Biomaterials and Advanced Drug Delivery Laboratory, Stanford School of Medicine, Stanford,
14 CA 94304, USA
15
16
17
18
19
20
21
22

23
24 *Corresponding Author

25 Tulio A Valdez M.D., MSc

26
27 Department of Otolaryngology and Head and Neck Surgery (OHNS)

28
29 Stanford University School of Medicine, CA, 94305, USA
30

31 Phone: + 1 (650) 724-4800
32

33 Fax: +1 (650) 721-2163
34

35 Email: tvaldez1@stanford.edu
36
37
38
39
40
41
42
43
44
45
46
47
48
49
50
51
52
53
54
55
56
57
58
59
60

Abstract

The tympanic membrane (TM) is a dynamic structure that separates the middle ear from the external auditory canal. It is also integral for the transmission of sound waves. In this study, we demonstrate the feasibility of using Raman spectroscopy to identify early chemical changes resulting from inflammation in the TM that can serve as an indicator of acute otitis media. Bacterial lipopolysaccharide (LPS) was injected trans-tympanically in a murine model. Presence of inflammatory response was assessed with binocular microscopy, confirmed with histopathology and immunofluorescence staining. Successful discrimination suggesting spectral differences among the control and LPS treated groups was achieved using principal component analysis. Raman imaging revealed major differences in collagen distribution and nucleic acid content. Image segmentation analysis on the trichrome stained tissue sections was performed to corroborate the Raman spectra. The spectral co-localization study suggests changes in the expression of collagen IV specific signals in LPS treated samples. The overall findings of the study support prospective application of RS in the diagnosis and therapeutic monitoring of otitis media.

Keywords: Raman spectroscopy, Imaging, Otitis Media, Tympanic Membrane, Collagen

Introduction

The ear is one of the most important sensory organs of the human body [1]. In addition to its function as an acoustic organ, it is also responsible for maintaining equilibrium. The ear is divided into three major components: the external, middle, and inner ear. The tympanic membrane (TM, eardrum, membrana tympani) is part of the middle ear and serves as a boundary with the external ear. Other major components of the middle ear include ossicles and the Eustachian tube [1-4]. Sound transmission is the primary function of middle ear components including the TM. Sound waves traveling across the external ear canal induce vibrations in the TM. These vibrations coupled with minor amplifications then get transferred to cochlear fluid and finally to hair cells. The ability of the TM to withstand large pressure fluctuations has been primarily credited to the remarkable arrangement of the solid collagen fibers [5,6].

Otitis media (OM) is one of the most commonly observed disease conditions of the middle ear. It is estimated that ~85% of children will have experienced an episode of OM before 5 years of age [7]. OM is also the most common indication for prescribing antibiotics and for surgery in pediatric patients under the age of 15 [7]. Acute otitis media (AOM), most commonly referred as an ear infection, occurs due bacterial and viral infections and is an important variant of otitis media. Undiagnosed otitis media can lead to extracranial and intracranial complications such as hearing loss, meningitis, facial nerve paralysis, and brain abscesses [8,9]. Changes in the stiffness of the TM in experimental models of otitis media have been previously reported [10]. Collagen fibers of the lamina propria form the backbone of the TM providing it with the required tensile strength and rigidity. Long term infection and inflammation in the TM can lead to a shift towards less deformation-resistant collagen type [11]. Development of cholesteatoma, a noncancerous but highly destructive and recurrent growth has also been connected with disruption in the lamina propria [12]. It is also reported that in pediatric patients who are susceptible to repeated ear infections, the TM tends to be weaker and prone to rupture due to disturbances in the collagen structure [5]. The repeated assaults in the form of inflammation on the structural integrity of the TM can significantly reduce its strength and cause the subsequent development of sequelae. Clinicopathological features of the TM in these conditions have been previously reported [5,10]. Steinfeldt *et al* performed a detailed study using immunohistochemistry (IHC) and electron

1
2
3 microscopy (EM) to explore changes in specific collagen type associated with AOM and
4 myringotomy [5].
5
6

7 Photonic approaches for improving the diagnosis of middle ear diseases have been explored
8 widely. These include the application of auto fluorescence, multicolor reflectance [13], diffuse
9 reflectance spectroscopy [14], optical coherence tomography [15–18] and short-wave infrared
10 imaging (SWIR) [19] to improve the OM diagnosis. Among the widely used photonic techniques,
11 Raman spectroscopy (RS) maintains an upper hand as it offers a non-ionizing, label-free, and non-
12 destructive tool for molecular characterization of the biological specimens. It is based upon the
13 inelastic scattering of light. Interaction of light with the molecular vibrations of a specimen
14 generates unique shifts of molecules within its native context. It has been applied extensively both
15 under *in vivo* and *ex vivo* conditions to study molecular level changes associated with disease
16 occurrence or therapeutic intervention [20-23]. We recently reported that RS can be used to
17 differentiate between middle ear effusion specimens and pathologies [24, 25].
18
19
20
21
22
23
24
25
26

27 Histopathology, IHC, and EM are the main tools employed for studying changes in the TM in
28 response to a pathological condition. However, these methods suffer from limitations in terms of
29 time consumption, inter-observer subjectivity, and destructive nature. In the present study, we
30 evaluated the efficacy of RS in identifying inflammation-induced changes in the TM in a label-
31 free manner using a murine model.
32
33
34
35

36 Materials and Methods

37 *Animal model and lipopolysaccharide (LPS) treatment*

38
39 Female C57BL/6J mice (4–6 weeks old) were purchased from Jackson Laboratory (Bar Harbor,
40 ME, USA). All procedures were approved by the Administrative Panel on Laboratory Animal Care
41 (APLAC), Stanford University (protocol number-APLAC-33028). The animals were anesthetized
42 with an intraperitoneal injection of ketamine (100 mg/kg) and xylazine (10 mg/kg). Three (3) μ l
43 LPS (L7261-Sigma) emulsion was administered through trans-tympanic injection in the left ear.
44 The stock solution of LPS at a concentration of 20 mg/ml was prepared in 0.9% sodium chloride.
45 The right ear was untreated and served as a control.
46
47
48
49
50
51
52

53 *Sample collection and histopathology*

1
2
3 Mice were kept alive for a period of 72 hours and the progress of otitis media was monitored
4 visually. Mice were sacrificed by cervical dislocation and the middle ear was harvested. Samples
5 were fixed in 4% paraformaldehyde (PFA) overnight at 4°C, rinsed with phosphate buffer saline
6 (PBS) of pH 7.3 to remove residual traces of PFA. This was followed by decalcification of samples
7 using Decal Overnight Bone Decalcifier (Decal chemical corporation, Tallman, NY) solution.
8 Tissues were rinsed free of any decalcifier solution by multiple washes using PBS and embedded
9 using OCT freezing medium. Sequential frozen tissue sections of thickness 10 µm and 7 µm were
10 collected for Raman imaging and histopathology, respectively. For Raman imaging, sections were
11 collected on quartz slides (Alfa Aesar, 42297).

19 *Immunostaining*

21 For immunostaining, the harvested ear specimens were incubated in 30% sucrose in PBS at 4°C
22 overnight followed by serial incubation in sucrose and optimal cutting temperature (OCT)
23 compound mixture. Seven (7) µm sections on super frost slides (MAT1) were obtained from these
24 blocks and stored at -80°C until used. The slides were washed with PBS to remove OCT and were
25 then incubated for 2 hours in blocking reagent containing 10% normal goat serum
26 (Thermofisher, 50197Z) and 0.3% Triton X-100 prepared in PBS. Incubation in primary antibody
27 Isolectin GS-IB4 (Thermofisher, I21412, 1:2000) diluted in blocking reagent was carried out at
28 4°C for 24 hours. Sections were then washed in PBS containing 0.1% Triton x100 and incubated
29 with Alexa Fluor 488 at 37°C for 1 hour (Thermofisher, A-11006, 1:100) and GS-IB4 conjugated
30 to Alexa Fluor 568. Finally, tissues were washed twice in PBS containing 0.1% Triton X100 and
31 1x in PBS, mounted (Vector Labs, H-1000), coverslipped (VWR, 631-0136), and visualized under
32 a Zeiss laser-scanning microscope 700 (LSM 700).

42 *Raman imaging*

44 Raman mapping (n=5) was performed using Horiba Xplora spectrometer coupled with a 50X
45 objective (Olympus, NA=0.80), 600 gr/mm grating, and 785 nm excitation. Maps from three
46 consecutive sections were generated from each animal. Region of interest was chosen under the
47 guidance of H&E stained sections. Typical exposure time at every point of the collection was 5
48 seconds and the spectra were acquired with 1 µm spatial resolution. Spectral pre-processing steps
49 such as spectral interpolation, cosmic removal, unit normalization, and Principal Component
50 Analysis (PCA) were performed using in-house MATLAB based codes [25]. For background
51
52
53
54
55
56
57
58
59
60

1
2
3 corrections spectrum obtained from OCT was subtracted followed by fitting of 4th order
4 polynomial function. Raman mapping using typical bands corresponding to collagen, DNA, and
5 phenylalanine were performed to understand the inflammation-induced changes in the TM.
6
7 Average band intensity across 30 Raman maps (15-control and 15-LPS treated) was computed by
8
9 generating a mean of area under each of the above mentioned Raman bands.
10
11

12 *Masson's Trichrome Staining*

13

14
15 The tissue sections obtained from the sucrose gradient processed tissue blocks were rehydrated
16 through serial alcohol wash. The sections were fixed in Bouin solution at 60°C and stained in
17 Weigert's hematoxylin solution for 10 minutes. This was followed by washing and staining with
18 Biebrich scarlet-acid fuchsin solution. Differentiation of the tissue slices was performed using
19 phosphomolybdic-phosphotungstic acid solution. The slides were then transferred to aniline blue
20 followed by acetic acid solution. The final step included rehydration with alcohol, clearing in
21 xylene, and mounting in the resinous medium. Bright-field images of stained control and LPS-
22 treated (n=10) specimens were obtained at x40 magnification. Total collagen content in these
23 specimens was quantified using Fiji (ImageJ, NIH) software. Masson's trichrome stain vector in
24 the color deconvolution plugin was applied to each image and the red, blue, and green channels
25 were separated. Collagen can be observed in both blue and green channels post deconvolution. For
26 this analysis, the green channel images were chosen as they do not have nuclei. The entire TM
27 region under the green channel served as a region of interest (ROI) and threshold value was
28 adjusted manually. Area fraction option was specifically used to record the percentage of the area
29 within the traced selection. Finally, the amount of collagen was computed using the ROI manager
30 tool as a measure of area fraction.
31
32
33
34
35
36
37
38
39
40
41
42

43 Statistical Analysis

44

45 Unpaired student's 't' test coupled with Welch correction using GraphPad PRISM (v.8.1.2) was
46 performed to assess the level of significance in all the experiments.
47
48

49 Results

50

51
52 In the first step, the influence of the used LPS concentration on the structural integrity of the TM
53 was evaluated. As shown in Fig 1, a significant increase in the width of the TM due to LPS
54 treatment was observed. The histopathology also revealed infiltration of cells along with epithelial
55
56
57
58
59
60

1
2
3 proliferation. In order to confirm if these cells are activated macrophages induced by LPS
4 treatment, immunostaining was performed. Activated macrophages display a terminal
5 galactopyranosyl group at their membrane surface that can bind to the lectin IB4. Staining with an
6 antibody coupled with a fluorophore (Alexa Fluor) can confirm the accumulation of activated
7 macrophages in the TM [26]. Red spots shown in Fig 1C suggest positive staining of activated
8 macrophages in the TM. The uniform structure of the TM in control specimens is also visible.
9

10
11
12
13
14 After confirming the presence of inflammatory signatures in the TM due to LPS treatment, Raman
15 imaging was performed to understand the changes at the biochemical level. The average spectrum
16 obtained from 5 tissue samples is shown in Fig 2. Visible spectral differences in bands
17 corresponding to collagen (856 cm^{-1}), CH_2 bending (1450 cm^{-1}), phenylalanine (1004 cm^{-1}),
18 nucleic acid (1576 cm^{-1}) and amide I (1660 cm^{-1}) were observed. The overall intensity of these
19 biochemical constituents was high in LPS treated mice as compared to the control, Fig 4. Peak
20 assignments were based upon existing literature [27,28]. Discrimination among the two groups
21 was achieved using Principal Component Analysis (PCA). Scatter plot generated by using score
22 of 2 and 3 is shown in Fig 2B. Spectral mapping using these bands was performed to explore their
23 distribution across the area of acquisition. As shown in Fig 3, the average collagen content and
24 hypercellularity (nucleic acid content) were high in LPS treated samples with respect to controls.
25 Statistically significant differences were observed across all five tissues, Fig 4. Collagen related
26 changes were further confirmed by Masson's Trichrome staining. A significantly higher fraction
27 of stained collagen fibers was found in LPS treated samples, Fig 5. Furthermore, to differentiate
28 between specific collagen types expressed in the TM, intensity of Raman bands corresponding to
29 collagen IV specific proline and phenylalanine amino acids was computed. The proline content
30 was found to be higher in LPS treated samples. This observation was further verified by calculating
31 the intensity ratio of bands assigned to proline-rich (1246 cm^{-1}) and proline poor (1271 cm^{-1})
32 collagen region originating from the amide III area [27,28]. As can be seen from Fig 4, this ratio
33 was found to be significantly higher in LPS treated samples. A Raman band around 1004 cm^{-1} has
34 been assigned to the ring breathing mode of phenylalanine amino acid. Strong intensity of this
35 band in the LPS treated samples indicate a higher amount of collagen IV, Fig 3G, H. Statistically
36 significant differences across 5 tissue samples were observed, Fig 4E. Spectral map generated
37 using the intensity of this band indicates higher intensity in LPS treated samples with respect to
38 controls, Fig 3G,H. To further verify if the higher intensity of phenylalanine band has its origin in
39
40
41
42
43
44
45
46
47
48
49
50
51
52
53
54
55
56
57
58
59
60

1
2
3 the areas with high amount of collagen shown in Fig 3E, F image fusion using three-color scheme
4 was performed. Areas with high intensity of the polypeptide backbone (856 cm^{-1}) are shown in
5 green. The areas with strong phenylalanine band are in red. The yellow indicates areas with similar
6 intensity. As shown in Fig 6, LPS treated samples have relatively large area with overlapping
7 intensities, suggesting a large amount of collagen, in this case, collagen type IV.
8
9

12 Discussion

13
14
15 The most common pathogens implicated in OM include both gram-positive bacteria such as
16 *Streptococcus pneumoniae* and other *Streptococcus species*, as well as gram-negative bacteria such
17 as *Haemophilus influenzae* [29]. LPS is a major component of the outer membrane of gram-
18 negative bacteria. It is known to activate macrophages and initiate the release of inflammatory
19 cytokines such as interleukin (IL)-1, IL-6, and tumor necrosis factors- α . It is well established that
20 LPS toxins injected in the middle ear can pass through the round window and cause inflammation
21 in the inner ear as well [30]. Early identification of these changes can provide vital clues about the
22 disease etiopathology and may help to design novel therapeutic strategies.
23
24
25
26
27
28

29
30 TM is the only membrane in the human body that is both semi-translucent and surrounded by air
31 on both sides under normal conditions [2]. It provides a window to the middle ear and anatomically
32 it can be divided into two parts, pars tensa, and pars flaccida. They mainly differ in the arrangement
33 of the collagen fibers and the presence of mast cells in the pars flaccida [3]. The TM consists of
34 three different layers: an outer epidermis, middle lamina propria, and the inner mucosal epithelial
35 layer of cuboidal, non-ciliated cells. A thin, keratinizing epithelium is the main constituent of the
36 epidermal layer. Lamina propria of the pars tensa region is rich in collagen fibers in both radial
37 and circular arrangements. During an OM episode, especially when there is a rupture or
38 perforation, there are changes in the collagen-rich layer especially in the distribution of the fibers
39 [30-32]. An increase in the thickness of the TM is an indication of disturbances in the overall
40 collagen profile. The histopathology of LPS treated ear specimens shown in Fig 1, indicate
41 increased thickness and infiltration with a large population of inflammatory cells confirming the
42 occurrence of AOM. These cells, especially macrophages, play a very important role in
43 maintaining cellular homeostasis. Most often they serve as the first line of defense and their
44 presence is considered a hallmark of infection. Under normal conditions, macrophages do not
45 display galactopyranosyl groups on their membranes and therefore they do not bind to Alexa Fluor
46
47
48
49
50
51
52
53
54
55
56
57
58
59
60

1
2
3 568 conjugated–GS-IB4 antibody, Fig 1C. However, after 72 hours of LPS stimulation, they start
4 displaying these terminal groups at their surface. Positive staining of activated macrophages shown
5 in Fig 1 further confirms the presence of AOM in our murine model.
6
7

8
9 Raman imaging can provide considerable details about the biochemical changes in response to
10 disease onset and progression. One of the biggest benefits of Raman imaging is its ability to
11 provide molecular-level information in a label-free manner. A study by Jonas *et al.* showed that
12 RS can provide in-depth information about changes in the biochemical milieu of tissues in
13 response to drug treatment [33]. Average spectrum suggests major changes in the overall collagen
14 content of the tissue, Fig 2. Origin of Raman band around 856 cm^{-1} has been assigned to the proline
15 ring in the collagen polypeptide chain [27,28,34]. The band around 1450 cm^{-1} originates from CH_2
16 bending deformation of collagen, protein, and lipids. Enhanced intensity of these bands in the LPS
17 treated samples indicate higher collagen content. Hyper cellularity was confirmed by the enhanced
18 intensity of nucleic acid band originating from C-N stretch of guanine nucleotide (1576 cm^{-1}) [27].
19 Principal Component Analysis is one of the most widely utilized tools for data overviewing and
20 outlier identification [23]. Scatter plot generated using principal component 2 (35.9%) and 3
21 (2.1%) yielded slightly overlapping clusters, Fig 2. This can be attributed to the presence of
22 analogues areas in both groups. This is expected during early stages of AOM. Principal component
23 1 was not used for classification had no diagnostic features , even though had the highest
24 contribution (46%) to the overall variance was not used, in it. The middle layers of both ‘pars tensa
25 and pars flaccida’ regions of the TM are composed of collagen fibers that provide rigidity to the
26 TM. The spectral map shown in Fig 3a and 3E is suggestive of the uniform distribution of the
27 collagen fibers in the control samples, however, this was disturbed in the case of LPS treated
28 specimens, Fig 3b and 3f. Corroborating with the differential features noted in the average spectra
29 average intensity bands at 1450 and 856 cm^{-1} were significantly higher in LPS treated samples. A
30 closer look at the spectral map generated using DNA band (Fig 3c) suggest infiltration with a large
31 number of cells in the TM, corroborating with the immunostaining findings. The origin of localized
32 enhanced intensity in the control specimen can be assigned to the presence of mast cells in the pars
33 flaccida region. Increase in collagen content was further validated with Masson’s trichrome
34 staining, which is one of the widely used methods in clinics for collagen content estimation.
35 Briefly, this staining process consists of three different dyes specific for muscles, collagen fibers,
36 fibrin and blood cells [35]. Biebrich scarlet-acid fuchsin solution stains all acidophilic tissue
37
38
39
40
41
42
43
44
45
46
47
48
49
50
51
52
53
54
55
56
57
58
59
60

1
2
3 elements such as cytoplasm, muscle, and collagen red. Serial washing with phosphomolybdic-
4 phosphotungstic solution as a decolorizer leads the dye to diffuse out of the collagen fibers due to
5 their small size. Finally, aniline blue is used to stain the collagen fibers. As mentioned the
6 percentage of blue color (collagen content) across the whole section was significantly higher in
7 LPS treated samples, Fig 5.
8
9

10
11
12 Collagen is considered the most abundant protein of the human body [36]. There are more than 20
13 different types of collagen depending upon the specific tissue type. Typical structure collagen
14 consists of a backbone made up of 3 polypeptide chains coiled around each other and stabilized
15 mainly by proline and glycine amino acids. This triple helical structure further combines together
16 to form collagen fibrils and later fibers of several micrometer diameters [36]. The composition and
17 structure of collagen fibers in the TM had been studied in great detail using electron microscopy
18 [37, 38]. Knutsson *J et al* has reported that collagen type I, II, III, and IV can be commonly found
19 in the healthy TM. They further suggest that the ratio of these collagen types' changes depending
20 upon the pathological state [4, 11]. Steinfeldt *et al.* have also reported that the collagen content of
21 the TM is modified during inflammation or perforation healing [5]. IHC based studies had revealed
22 that type II collagen is most common in lamina propria under normal conditions [39]. This
23 observation is further supported by the occurrence of collagen II-associated Meniere's disease and
24 otosclerosis in the ear [40]. Collagen IV is abundant in the basement membrane. As mentioned,
25 repeated exposure of the TM to inflammatory events can negatively affect its strength by
26 disturbing the distribution of the collagen fibers. For example, in patients with chronic OM with
27 effusion, the TM may get retracted towards the middle ear leading to a collapse and complete loss
28 of collagen. In the next step, we attempted to understand changes in specific collagen type due to
29 LPS treatment. Glycine, proline, and hydroxyproline are the most abundant amino acids in
30 collagen and are involved mainly in cross-linking and stabilizing the structure. Previous studies
31 have reported that collagen IV can be characterized by interruptions in the polypeptide backbone
32 and in the presence of disulfide linkages [41]. Nguyen *et al* demonstrated that differences in the
33 phenylalanine regions along with proline and hydroxyproline amino acid content could serve as a
34 reliable Raman spectroscopic marker to differentiate between collagen I and IV in the skin [42].
35 The significant differences observed in relative intensity of proline and phenylalanine Raman
36 bands suggests the presence of a large amount of collagen IV in LPS treated samples as compared
37 to control, Fig 4D, E. This observation is further corroborated by image fusion study. In computer
38
39
40
41
42
43
44
45
46
47
48
49
50
51
52
53
54
55
56
57
58
59
60

1
2
3 vision, fusion is defined as a process of combining multiple images to generate a single image with
4 accurate spatial information. We hypothesize if the LPS treated samples have a higher amount of
5 collagen IV, Raman band intensities of phenylalanine band should spatially overlap with the areas
6 with high collagen content shown in Fig 3E, F. A blended overlaid image was created to
7 demonstrate areas with similar intensity. The red color was chosen for phenylalanine, green was
8 chosen for polypeptide backbone and the color yellow represents areas with similar intensity
9 between two images. The presence of a large area in yellow color in Fig 6B, confirms predominant
10 collagen IV specific signals in LPS treated samples.
11
12
13
14
15
16

17 While this proof-of-concept study is limited by the relatively small number of animals, it provides
18 novel insights into identifying the presence of AOM through changes in the TM. Our future studies
19 will focus on translating these observations for *in vivo* measurements using a fiber-optic probe.
20 The wealth of information and high order of segmentation provided by Raman images can be used
21 to generate novel diagnostic and prognostic markers associated with middle ear diseases. We
22 envision that objectivity, as well as the ability to provide information without any external agents,
23 will be attractive for augmenting several biomolecular and phenotyping studies especially related
24 with ear diseases.
25
26
27
28
29
30
31
32
33

34 Conclusions

35
36 The TM serves as a barrier and provides protection to the middle ear. Deformity in the structural
37 or architectural arrangement of its collagen fibers can lead to the spreading of infection to the inner
38 ear and ultimately may lead to hearing loss. Overall findings of our study suggest that an increase
39 in the ratio of collagen IV to collagen II can be considered as a potential spectroscopic marker for
40 detecting the presence of AOM. Future studies will focus on validating these markers to study
41 otitis media progression and assessing the therapeutic response or degree of AOM reversal.
42
43
44
45
46
47
48
49
50
51

52 Conflicts of Interest

53
54
55 None declared
56
57
58
59
60

1
2
3
4
5
6 Acknowledgments
7

8 The authors would like to acknowledge Doreen Wu from Stanford Animal Histology Services for
9 help with preparation of histologic specimens. Part of this work was performed at the Stanford
10 Nano Shared Facilities (SNSF), supported by the National Science Foundation under award ECCS-
11 1542152.
12
13
14
15
16
17
18
19
20
21
22
23
24
25
26
27
28
29
30
31
32
33
34
35
36
37
38
39
40
41
42
43
44
45
46
47
48
49
50
51
52
53
54
55
56
57
58
59
60

1
2
3 Figure Legends
4
5
6

7 Figure 1: LPS induced changes in the tympanic membrane (A) Histology images (B) Changes in
8 the width of the TM (N=11). The error bars represent standard deviation. (C) Immunostained
9 images of the TM stained with GS-IB4-AF 568 + AF 488 antibody. (* Statistically Significant)
10

11 Figure 2: (A) Average spectrum obtained from control and LPS treated samples (shaded area
12 indicates the standard deviation). Spectra has been vertically offset for better visibility. (B) PCA
13 scatter plot (C) Loading plot of principal components 2 and 3 used for PCA.
14
15

16 Figure 3: Figure 3: Spectral mapping using normalized intensity of Raman bands corresponding
17 to (A,B) CH₂ bending (1445 cm⁻¹), (C,D) Nucleic acid (1576 cm⁻¹), (E,F) Collagen polypeptide
18 backbone (856 cm⁻¹), (G,H) Phenylalanine (1004 cm⁻¹).
19

20 Figure 4: Mean band intensity of (A) CH₂ bending (1445 cm⁻¹), (B) Nucleic acid (1576 cm⁻¹), (C)
21 Collagen polypeptide backbone (856 cm⁻¹), (D) ratio of proline-rich (1246 cm⁻¹) and proline poor
22 (1271cm⁻¹) and (E) Phenylalanine (1004 cm⁻¹). Data is presented as mean with standard error. (#
23 non-significant, * statistically significant)
24
25

26 Figure 5: (A) Masson's trichrome stained tympanic membrane from control and LPS treated mice
27 (B) Positively stained area of the whole section represented as the percentage of total area. The
28 error bars represent standard deviation. (* Statistically Significant)
29

30 Figure 6: Fused images using intensity of collagen backbone (green, 856 cm⁻¹) and collagen IV
31 specific phenylalanine (red, 1004 cm⁻¹) Raman bands. Areas with similar intensity are marked in
32 yellow.
33
34
35
36
37
38
39
40
41
42
43
44
45
46
47
48
49
50
51
52
53
54
55
56
57
58
59
60

References

1. J. C. Luers and K. B. Huttenbrink, *Journal of anatomy*, 2016, 228, 338-353.
2. J. Sade and M. Luntz. *Ann Otol Rhinol Laryngol*, 1990,99,529-34.
3. S. Dogru, A. Haholu, A. Gungor, Z. Kucukodaci, H. Cincik, T. Ozdemir, and H. Sen, *Otolaryngology--head and neck surgery: official journal of American Academy of Otolaryngology-Head and Neck Surgery*, 2009, 140, 177-182.
4. J. Knutsson, D. Bagger-Sjoback and M. von Unge, *Otology & neurotology: official publication of the American Otological Society, American Neurotology Society [and] European Academy of Otology and Neurotology*, 2009, 30, 1225-1229.
5. K. Steinfeldt, C. Johansson, and S. Hellstrom, *Archives of otolaryngology-head & neck surgery*, 2006, 132, 293-298.
6. J. Hartwein, K. Mensing, G. Schaeg and H. W. Pau, *Laryngo- rhino- otologie*, 1990, 69, 333-336.
7. M. M. Rovers, A. G. Schilder, G. A. Zielhuis and R. M. Rosenfeld, *Lancet*, 2004, 363, 465-473.
8. S. Pirozzo and C. Del Mar, *The Western journal of medicine*, 2001, 175, 402-407.
9. R. M. Rosenfeld, *International journal of pediatric otorhinolaryngology*, 2002, 64, 89-95.
10. M. von Unge and D. Bagger-Sjoback, *The American journal of otology*, 1994, 15, 663-669.
11. J. Knutsson, D. Bagger-Sjoback and M. von Unge, *Otology & neurotology: official publication of the American Otological Society, American Neurotology Society [and] European Academy of Otology and Neurotology*, 2007, 28, 486-491.
12. B. Ars, W. De Craemer, and N. Ars-Piret, *Clinical otolaryngology and allied sciences*, 1989, 14, 471-475.
13. T. A. Valdez, R. Pandey, N. Spegazzini, K. Longo, C. Roehm, R. R. Dasari and I. Barman, *Analytical chemistry*, 2014, 86, 10454-10460.
14. T. A. Valdez, N. Spegazzini, R. Pandey, K. Longo, C. Grindle, D. Peterson and I. Barman, *Analytical and bioanalytical chemistry*, 2015, 407, 3277-3283.
15. M. Sundberg, M. Peebo, P. A. Oberg, P. G. Lundquist, and T. Stromberg, *Physiological measurement*, 2004, 25, 1473-1483.
16. C. T. Nguyen, W. Jung, J. Kim, E. J. Chaney, M. Novak, C. N. Stewart, and S. A. Boppart, *Proceedings of the National Academy of Sciences of the United States of America*, 2012, 109, 9529-9534.
17. G. L. Monroy, P. Pande, R. M. Nolan, R. L. Shelton, R. G. Porter, M. A. Novak, D. R. Spillman, E. J. Chaney, D. T. McCormick, and S. A. Boppart, *Journal of biomedical optics*, 2017, 22, 1-11.
18. G. L. Monroy, P. Pande, R. L. Shelton, R. M. Nolan, D. R. Spillman, Jr., R. G. Porter, M. A. Novak, and S. A. Boppart, *Journal of biophotonics*, 2017, 10, 394-403.
19. J. A. Carr, T. A. Valdez, O. T. Bruns, and M. G. Bawendi, *Proceedings of the National Academy of Sciences*, 2016, 113, 9989.

- 1
- 2
- 3
- 4 20. L. A. Austin, S. Osseiran and C. L. Evans, *The Analyst*, 2016, 141, 476-503.
- 5 21. H. H. Mantsch, *The Analyst*, 2013, 138, 3863-3870.
- 6 22. N. M. Ralbovsky and I. K. Lednev, *Spectrochimica acta. Part A, Molecular and*
- 7 *biomolecular spectroscopy*, 2019, 219, 463-487.
- 8 23. S. P. Singh, S. Kang, J. W. Kang, P. T. C. So, R. R. Dasari, Z. Yaqoob and I. Barman,
- 9 *Scientific reports*, 2017, 7, 10829.
- 10 24. R. Pandey, S. K. Paidi, J. W. Kang, N. Spegazzini, R. R. Dasari, T. A. Valdez and I.
- 11 *Barman, Scientific reports*, 015, 5, 13305.
- 12 25. R. Pandey, C. Zhang, J. W. Kang, P. M. Desai, R. R. Dasari, I. Barman and T. A. Valdez,
- 13 *Journal of biophotonics*, 2018, 11, e201700259.
- 14 26. J. H. Zhang, S. L. Chen, Z. Q. Hou, J. Cai, M. M. Dong and X. R. Shi, *PloS one*, 2015, 10.
- 15 27. Z. Movasaghi, S. Rehman and I. U. Rehman, *Appl Spectrosc Rev*, 2007, 42, 493-541
- 16 28. F. S. Parker, *Applications of Infrared, Raman and Resonance Raman Spectroscopy in*
- 17 *Biochemistry*, Plenum Press, Newyork and London, 1983
- 18 29. S. S. Khoramrooz, A. Mirsalehian, M. Emaneini, F. Jabalameli, M. Aligholi, B. Saedi, A.
- 19 *Bazargani, M. Taherikalani, P. Borghaei and E. Razmpa, Auris Nasus Larynx*, 2012, 39,
- 20 369-373.
- 21 30. K. Hirose, S. Z. Li, K. K. Ohlemiller and R. M. Ransohoff, *Jaro-J Assoc Res Oto*, 2014,
- 22 15, 555-570.
- 23 31. Hermansson, K. Prellner, and S. Hellstrom, *Acta Oto-Laryngol*, 1990, 109, 421-430.
- 24 32. K. Magnuson, A. Hermansson and S. Hellstrom, *Ann Oto Rhinol Larynx*, 1996, 105, 397-
- 25 404.
- 26 33. O. Jonas, J. W. Kang, S. P. Singh, A. Lammers, F. T. Nguyen, R. R. Dasari, P. T. C. So,
- 27 *R. Langer and M. J. Cima, The Analyst*, 2018, 143.
- 28 34. K. Beck and B. Brodsky, *J Struct Biol*, 1998, 122, 17-29.
- 29 35. P. Hernandez-Morera, I. Castano-Gonzalez, C. M. Travieso-Gonzalez, B. Mompeo-
- 30 *Corredera and F. Ortega-Santana, PloS one*, 2016, 11.
- 31 36. M. J. Mienaltowski and D. E. Birk, *Adv Exp Med Biol*, 2014, 802, 5-29.
- 32 37. T. Shimada and D. J. Lim, *The Annals of otology, rhinology, and laryngology*, 1971, 80,
- 33 210-217.
- 34 38. T. Lildholdt, J. Clausen and E. I. Cantekin, *Journal of Laryngology and Otology*, 1983, 97,
- 35 785-791.
- 36 39. D. Broekaert, *Acta oto-rhino-laryngologica Belgica*, 1995, 49, 127-137.
- 37 40. T. Ishibe and T. J. Yoo, *The American journal of otology*, 1990, 11, 33-38.
- 38 41. R. Kalluri, *Nature reviews. Cancer*, 2003, 3, 422-433.
- 39 42. T. T. Nguyen, C. Gobinet, J. Feru, S. Brassart-Pasco, M. Manfait and O. Piot, *Spectrosc-*
- 40 *Int J*, 2012, 27, 421-427.
- 41
- 42
- 43
- 44
- 45
- 46
- 47
- 48
- 49
- 50
- 51
- 52
- 53
- 54
- 55
- 56
- 57
- 58
- 59
- 60

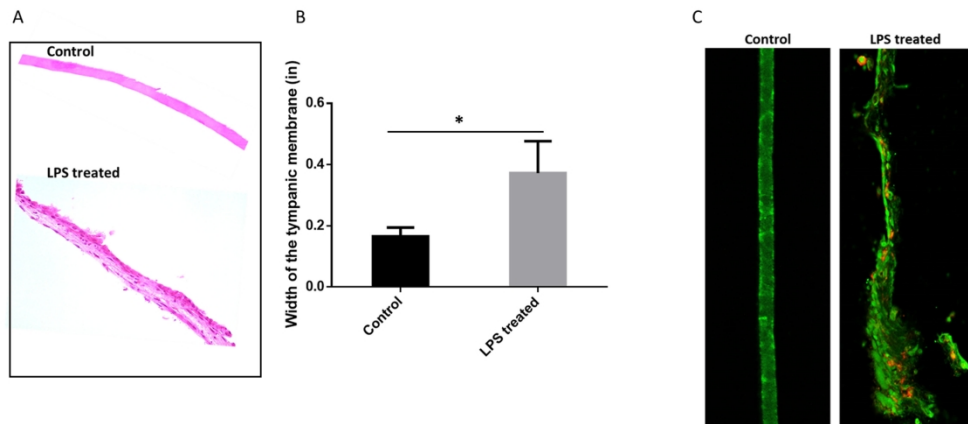


Figure 1: LPS induced changes in the tympanic membrane (A) Histology images (B) Changes in the width of the TM (N=11). The error bars represent the standard deviation. (C) Immunostained images of the TM stained with GS-IB4-AF 568 + AF 488 antibody. (* Statistically Significant)

314x141mm (300 x 300 DPI)

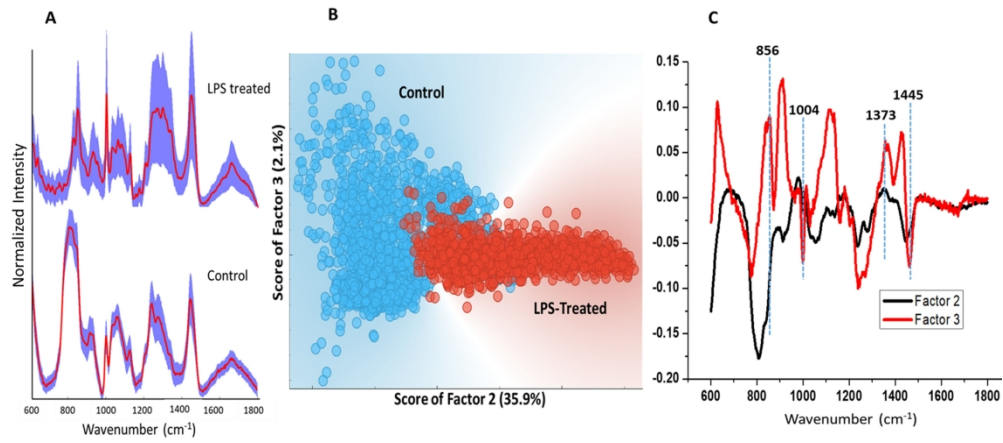


Figure 2: (A) Average spectrum obtained from control and LPS treated samples (shaded area indicates the standard deviation). Spectra have been vertically offset for better visibility. (B) PCA scatter plot (C) Loading plot of principal components 2 and 3 used for PCA.

321x145mm (300 x 300 DPI)

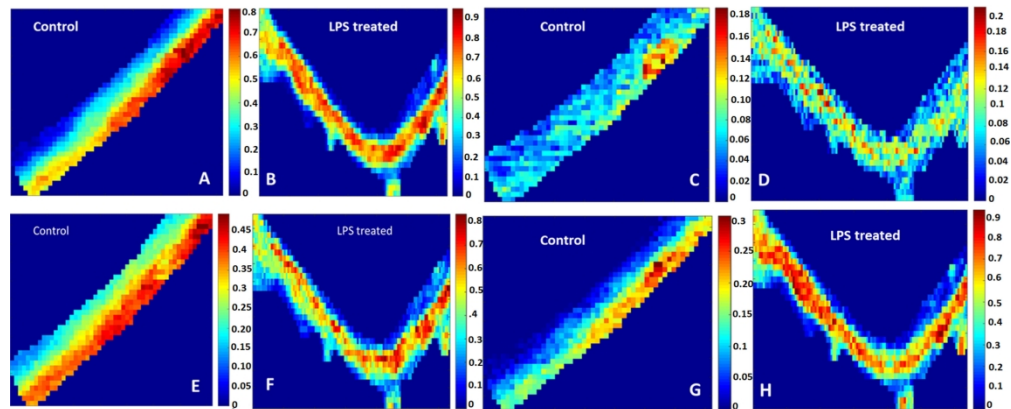


Figure 3: Figure 3: Spectral mapping using normalized intensity of Raman bands corresponding to (A,B) CH₂ bending (1445 cm⁻¹), (C,D) Nucleic acid (1576 cm⁻¹), (E,F) Collagen polypeptide backbone (856 cm⁻¹), (G,H) Phenylalanine (1004 cm⁻¹).

330x135mm (300 x 300 DPI)

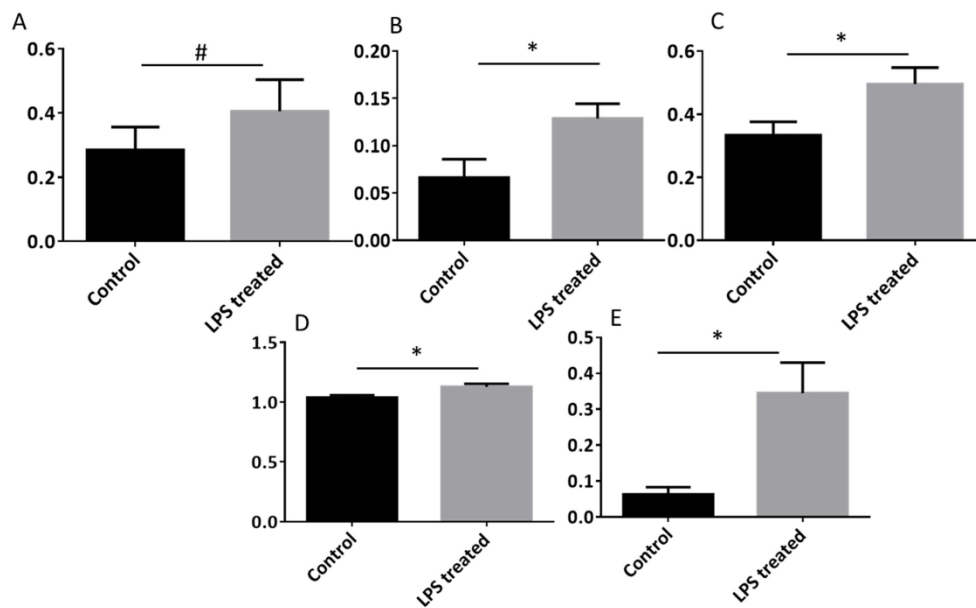


Figure 4: Mean band intensity of (A) CH₂ bending (1445 cm⁻¹), (B) Nucleic acid (1576 cm⁻¹), (C) Collagen polypeptide backbone (856 cm⁻¹), (D) ratio of proline-rich (1246 cm⁻¹) and proline poor (1271cm⁻¹) and (E) Phenylalanine (1004 cm⁻¹). Data is presented as mean with standard error. (# non-significant, * statistically significant)

248x156mm (300 x 300 DPI)

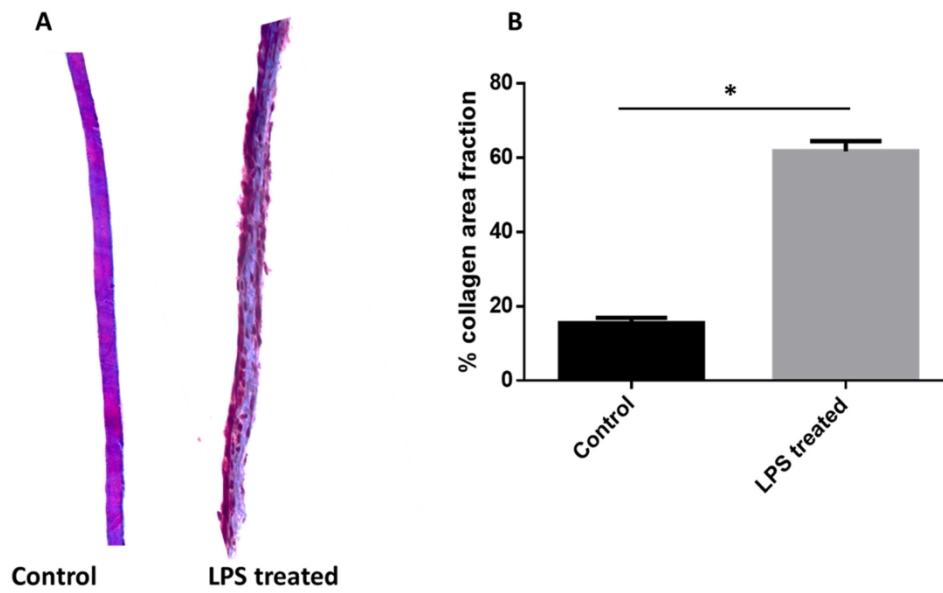


Figure 5: (A) Masson's trichrome stained tympanic membrane from control and LPS treated mice (B) Positively stained area of the whole section represented as the percentage of total area. The error bars represent standard deviation. (* Statistically Significant)

212x130mm (300 x 300 DPI)

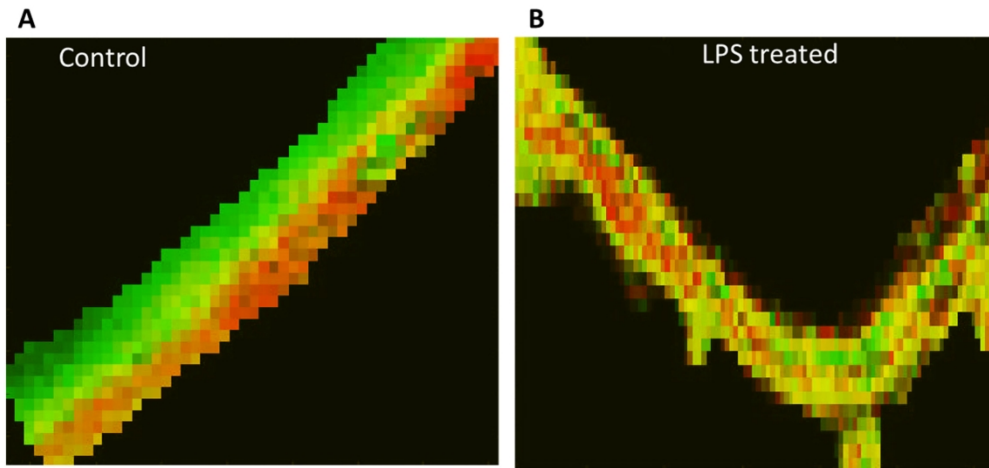


Figure 6: Fused images using intensity of collagen backbone (green, 856 cm⁻¹) and collagen IV specific phenylalanine (red, 1004 cm⁻¹) Raman bands. Areas with similar intensity are marked in yellow.

264x126mm (300 x 300 DPI)

1
2
3
4
5
6
7
8
9
10
11
12
13
14
15
16
17
18
19
20
21
22
23
24
25
26
27
28
29
30
31
32
33
34
35
36
37
38
39
40
41
42
43
44
45
46
47
48
49
50
51
52
53
54
55
56
57
58
59
60